Ultrastable heterodyne interferometer system using a CMOS modulated light camera

Rikesh Patel,* Samuel Achamfuo-Yeboah, Roger Light and Matt Clark

Applied Optics Group, Electrical Systems and Optics Research Division
University of Nottingham, University Park, Nottingham, NG7 2RD, UK

**eexrp4@nottingham.ac.uk*

Abstract: A novel ultrastable widefield interferometer is presented. This uses a modulated light camera (MLC) to capture and stabilise the interferogram in the widefield heterodyne interferometer. This system eliminates the contribution of piston phase to the interferogram without the need for common path optics and results in a highly stable widefield interferometer. The MLC uses quadrature demodulation circuitry built into each pixel to demodulate the light signal and extract phase information using an electronic reference signal. In contrast to the work previously presented [Opt. Express **19**, 24546 (2011)], the reference signal is derived from one of the pixels on board the MLC rather than an external source. This local reference signal tracks the instantaneous modulation frequency detected by the other pixels and eliminates the contribution of piston phase to the interferogram, substantially removing the contributions of unwanted vibrations and microphonics to the interferogram. Interferograms taken using the ultrastable system are presented with one of the interferometer mirrors moving at up to $85\,\mathrm{mm\,s^{-1}}$ over a variety of frequencies from 18 Hz to 20 kHz (giving a variation in optical path length of $220\,\mu$m, or 350 wavelengths at 62 Hz). This limit was the result of complex motion in the mirror mount rather than the stability limit of the system. The system is shown to be insensitive to pure piston phase variations equivalent to an object velocity of over $3\,\mathrm{m\,s^{-1}}$.

OCIS codes: (100.3175) Interferometric imaging; (110.3175) Interferometric imaging.

References and links

1. H. Osterberg, "An interferometer method of studying the vibrations of an oscillating quartz plate," J. Opt. Soc. Am. **22**, 19–34 (1932).
2. R. Patel, S. Achamfuo-Yeboah, R. Light, and M. Clark, "Widefield heterodyne interferometry using a custom CMOS modulated light camera," Opt. Express **19**, 24546–24556 (2011).
3. F. Ghebremichael and R. Knize, "Polymer relaxations determined by use of a temporally and thermally stable interferometer," Opt. Lett. **24**, 1481–1483 (1999).
4. K. Birch and M. Okaji, "Stable interferometer supporting system," J. Phys. E: Sci. Instrum. **19**, 361–363 (1986).
5. W. Lehmann, P. Gattinger, M. Keck, F. Kremer, P. Stein, T. Eckert, and H. Finkelmann, "Inverse electromechanical effect in mechanically oriented sc*-elastomers examined by means of an ultra-stable Michelson interferometer," Ferroelectr. **208**, 373–383 (1998).
6. H. Kikuta, S. Asai, H. Yasukochi, and K. Iwata, "Force microscopy using common-path optical-heterodyne interferometer," Jpn. J. Appl. Phys. Part 1 **30**, 587–590 (1991).
7. Y. Park and K. Cho, "Heterodyne interferometer scheme using a double pass in an acousto-optic modulator," Opt. Lett. **36**, 331–333 (2011).

#169402 - $15.00 USD Received 25 May 2012; revised 5 Jul 2012; accepted 9 Jul 2012; published 19 Jul 2012

8. N. A. Riza, M. A. Arain, and F. N. Ghauri, "Self-calibrating hybrid wavelength, polarization, and time-multiplexed heterodyne interferometers for angstrom precision measurements," Opt. Eng. **45**, 125603 (2006).
9. J. Chieh, S. Yang, H.-E. Horng, C.-Y. Hong, and H. Yang, "Measurements of the complex transmission/reflection coefficient of a material using mixed-type common-path heterodyne interferometery," IEEE Trans. Instrum. Meas. **58**, 1878–1885 (2009).
10. N. Sawyer, C. See, M. Clark, M. Somekh, and J. Goh, "Ultrastable absolute-phase common-path optical profiler based on computer-generated holography," Appl. Opt. **37**, 6716–6720 (1998).
11. M. J. Offside, M. Somekh, and C. See, "Common path scanning heterodyne optical profilometer for absolute phase measurement," Appl. Phys. Lett. **55**, 2051–2053 (1989).
12. M. Takeda and K. Mutoh, "Fourier transform profilometry for the automatic measurement of 3-D object shapes," Appl. Opt. **22**, 3977–3982 (1983).
13. R. Smythe and R. Moore, "Common path scanning heterodyne optical profilometer for absolute phase measurement," Opt. Eng. **23**, 361–364 (1984).
14. B. K. A. Ngoi, K. Venkatakrishnan, and N. R. Sivakumar, "Phase-shifting interferometry immune to vibration," Appl. Opt. **40**, 3211–3214 (2001).
15. P. Dmochowski, B. Hayes-Gill, M. Clark, J. Crowe, M. Somekh, and S. Morgan, "Camera pixel for coherent detection of modulated light," Electron. Lett. **40**, 1403–1404 (2004).
16. M. J. Griffin, "An introduction to whole body vibration," in *Handbook of Human Vibration*, (Academic Press, 1996), 27–42.
17. A. Ismail, M. Nuawi, N. Kamaruddin, and R. Bakar, "Comparative assessment of the whole-body vibration exposure under different car speed based on Malaysian road profile," J. Appl. Sci. **10**, 1428–1434 (2010).
18. C. Gordon, "Generic criteria for vibration-sensitive equipment," Proc. SPIE Int. Soc. Opt. Eng. **1619**, 71–85 (1992).
19. W. W. Hays (U.S.), *Facing Geologic and Hydrologic Hazards: Earth-Science Considerations* (U.S. Dept. of the Interior, Geological Survey, 1981).
20. P. Stafford, F. Strasser, and J. Bommer, "An evaluation of the applicability of the NGA models to ground-motion prediction in the Euro-Mediterranean region," Bull. Earthquake Eng. **6**, 149–177 2008.

1. Introduction

Interferometers are used for a wide variety of purposes, many of which only require the relative phase distribution across the field of view rather than the absolute phase. Most interferometers are sensitive to vibrations in any part of the optics which is not common path and this leads to problems with stability. If the optics of the interferometer or the position of the object is subject to any vibrations, they contribute a time varying phase term to the interferogram, where they shift the position of fringes in homodyne interferometers and the temporal phase of the signal in heterodyne interferometers. Normally the frequency of the vibrations is higher than the frequency of the interferometer read out so the net result of these unwanted vibrations is to reduce the fringe visibility (or temporal modulation depth) to $J_0\left(\frac{2\pi}{\lambda}A\right)$ of the intensity they would be in a stationary system (where λ is the wavelength of the light and A amplitude of optical path length (OPL) variations [1]). This equation indicates the first zero in the visibility occurs when the amplitude of vibration is ~ 1.2 wavelengths for normal incidence. Furthermore, the sign changes in the visibility for vibration amplitudes above this value, indicating an inversion of the fringe contrasts. For systems where the vibration is unknown, random, or time varying in frequency or amplitude, interpreting the fringes becomes more difficult for larger vibration amplitudes.

The work presented in this paper builds on previous work [2], which involved capturing widefield images of heterodyne interferograms modulated at 15 MHz. In this paper, we present a widefield ultrastable interferometer configuration using a prototype custom CMOS modulated light camera (MLC) which exhibits immunity to changes of piston phase. This provides a high level of immunity against vibrations or path length variations in the interferometer, or between the interferometer and the object. This immunity to piston phase variations renders the interferometer insensitive to the absolute path length meaning that it will only capture relative phase distributions.

#169402 - $15.00 USD Received 25 May 2012; revised 5 Jul 2012; accepted 9 Jul 2012; published 19 Jul 2012

1.1. *Existing stabilising techniques*

Other methods of stabilising an interferometric setup can be achieved by physically modifying the setup, including reducing environmental factors such as temperature changes and vibration [3], through the use of sensors and feedback into the system mirrors to counteract unwanted OPL changes [4, 5], or through the implementation of a largely common path system [6–11]. While these approaches can tackle the stability problems associated with unwanted vibrations, they can add unwanted complexity to the optics and may have limited effectiveness in terms of their immunity to vibrations of differing frequency and amplitude.

High speed acquisition methods can also compensate for vibration experienced on the system, making use of averaging to remove phase shifts as the pattern changes during capture [12]. However, the limit of immunity is dependant on the frame rate, requiring a quick acquisition time in large vibration situations. Polarisation fringe shifting techniques with simultaneous detection has similarities with the ultrastable system presented [13, 14]. Phase shifting, splitting, and mixing is done externally in the polarisation technique whilst the in the ultrastable interferometer this is done electronically and internally with the MLC.

1.2. *Modulated light capture*

The MLC used was fabricated as a custom camera chip using a 0.35 μm standard CMOS process. It has a 32×32 pixel array, with a fill factor of 16 % and a pixel pitch of 115 μm. Previous implementations of the camera included a single test pixel [15]. Information about accuracy and range have been explored previously [2] and further specification of the camera will be presented in future works. The MLC has demodulating circuitry at each pixel that simultaneous demodulates the in-phase and quadrature components of the time varying intensity of light incident upon it (see Fig. 1). It uses an electronic reference signal to accomplish the demodulation using two electronic mixers. It is capable of demodulating light modulated in the megahertz region (100 kHz-17 MHz), as well as being able to read out intensity and phase data simultaneously and continuously [15]. At 15 MHz, the maximum error in phase is measured to be $\pm$0.1 radians, giving a phase accuracy of 1.8 %. This prototype camera is of low resolution but is scalable to much higher resolutions.

2. Principle of operation

A heterodyne interference pattern is generated by interfering two light beams with different frequencies. The wave propagation equation in scalar form of two beams, $E_R(x,y,t)$ and $E_I(x,y,t)$, can be expressed as:

$$\begin{aligned} E_R(x,y,t) &= a_r \cos(\omega_r t + \phi_r(x,y) + \psi_r(t)) \\ E_I(x,y,t) &= a_i \cos(\omega_i t + \phi_i(x,y) + \psi_i(t)) \end{aligned} \quad (1)$$

where $\omega = 2\pi f$ and f is the optical frequency. In these equations, the waves travel in the same direction but have different frequencies, f. The phase is described by ϕ when determined by the spatial positioning and ψ when determined by time. The goal of keeping the system ultrastable is achieved by eliminating ψ. Time, amplitude and spatial coordinates are represented by t, a, x and y respectively.

When interference between these two beams occurs, a DC term, a frequency difference (beat frequency) term ($\omega_r - \omega_i$), and higher frequency terms (the sum frequency and double frequencies) are generated. The photodiode at each pixel will only detected the DC and difference frequency terms. The difference frequency term will also contain the difference in phases, which

#169402 - $15.00 USD Received 25 May 2012; revised 5 Jul 2012; accepted 9 Jul 2012; published 19 Jul 2012

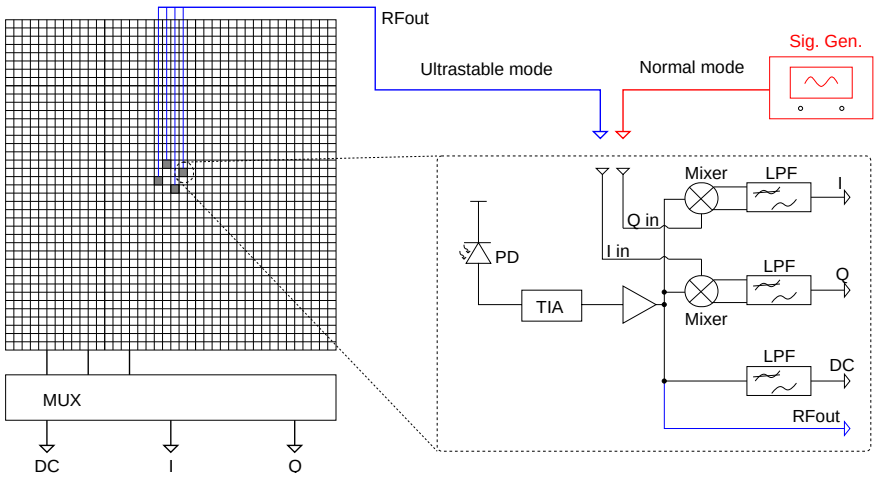

Fig. 1. A schematic of the MLC camera array and of an RFout pixel. Each pixel in the array contains a transimpedance amplifier to convert photocurrent into a voltage, an amplifier, in phase and quadrature mixers (Gilbert cells) and low phase filters (around 2 kHz) for the I, Q and DC outputs. Four pixels in the array contain additional circuitry that allows them to output the raw RF signal. In the normal mode of operation, the I and Q inputs are driven by a signal generator. In ultrastable mode, they are driven by signals derived from the RFout signal from one of the four special pixels.

include the position phase ($\phi_d = (\phi_r - \phi_i)$) and temporal phase ($\psi_d = (\psi_r - \psi_i)$). The intensity signal, $I = I(x,y,t)$, observed at each pixel can be expressed by:

$$I = I_{\rm dc} + I_{\rm RF} = I_{\rm dc} + A\cos(\omega_d t + \phi_d(x,y) + \psi_d(t)) \tag{2}$$

where $I_{\rm dc} = 1/2a_r^2 + 1/2a_i^2$, and $A = a_r a_i$. Each pixel on the MLC outputs raw DC intensity, $V_{\rm DCout}$, at this point by passing the signal through a low pass filter to remove $I_{\rm rf}$.

2.1. *Conventional operation*

In a perfectly stable system, the phase change dependant on time, ψ_d, would be zero. However, in a real system, this will vary (e.g. due to vibration). ψ_d is typically an unknown function of time and is difficult to predict or model. In order to get an ultrastable interferometer, it is necessary to reduce the effect of ψ_d to zero.

In the previous paper [2], the detected signal, I, was mixed with externally generated references, an in-phase, $i_{\rm lo}$, and a quadrature, $q_{\rm lo}$, signals, which have the same frequency as the beat frequency between the two beams, ω_d:

$$\begin{aligned} i_{\rm lo} &= B\cos(\omega_d t) \\ q_{\rm lo} &= B\sin(\omega_d t) \end{aligned} \tag{3}$$

It should be noted that the reference signals are externally derived and do not have the time varying phase component, ψ.

Mixing the detected signal, I, with the in-phase and quadrature signals and low pass filtering (see Fig. 1) to remove the AC components, produces the DC in-phase, $i_d(x,y)$, and quadrature, $q_d(x,y)$, outputs:

#169402 - $15.00 USD Received 25 May 2012; revised 5 Jul 2012; accepted 9 Jul 2012; published 19 Jul 2012

$$\begin{aligned} i_d(x,y) &= BA\cos[\phi_d(x,y)+\psi_d(t)] \\ q_d(x,y) &= BA\sin[\phi_d(x,y)+\psi_d(t)] \end{aligned} \tag{4}$$

This allows us to calculate the phase (with the time varying term) as:

$$\phi_d(x,y)+\psi_d(t) = \arctan\left(\frac{q_d}{i_d}\right) \tag{5}$$

This equation contains the temporally varying phase, $\psi_d(t)$, that causes the interferometer instability.

2.2. Ultrastable configuration

In this paper, the detected signal at all pixels is mixed with the RF signal from a single pixel instead of an externally derived reference (see Fig. 1). Considering the signal observed for the light detected at one of the RFout pixels:

$$I_{\text{pixel1}} = I_{\text{dc1}} + I_{\text{rfout}} = I_{\text{dc1}} + A_1\cos[\omega_d t + \phi_{d1} + \psi_{d1}(t)] \tag{6}$$

This signal has the same form for the detected light as for every other pixel (Eq. (2)), but as this RF pixel is in a static position on the array, there is no (x,y) dependence. The position phase, ϕ_{d1}, the amplitude, A_1, and DC component, I_{dc1}, for this single pixel all are now constants. There is still however, the temporal phase dependence, $\psi_{d1}(t)$. It can be seen that I_{rfout} from this equation has a similar form to Eq. (3). Therefore after extracting the RFout signal (through high pass filtering), phase splitting it into I and Q inputs, and mixing it with the detected signal for every pixel (analogous to the processes seen in Eq. (4)), then as a result, we can rewrite Eq. (5) as:

$$\phi_d(x,y)+\psi_d(t)-\phi_{d1}-\psi_{d1}(t) = \arctan\left(\frac{q_d}{i_d}\right) \tag{7}$$

Compared with the conventional system output, the addition phase terms $\psi_{d1}(t)$ and $\phi_(d1)$ are carried in from the reference signal detected at the single pixel. Assuming that the vibrations only give rise to piston phase variations then, by definition $\psi_{d1}(t) = \psi_d(t)$, and the measured phase, $\phi_d(x,y)$ becomes (remembering that ϕ_{d1} is a constant that can be removed post captured):

$$\phi_d(x,y) = \arctan\left(\frac{q_d}{i_d}\right) \tag{8}$$

which no longer contains the $\psi_d(t)$ term that is responsible for instability. In practice ψ_{d1} contains an additional term associated with the propagation delay through the electronics. Since this is a fixed time delay, the contribution to the phase is frequency dependant but as long as it is small (compared with the inverse of the maximum frequency) this constant term may be ignored.

3. Demonstration of ultrastable performance

We conducted two experiments to demonstrate the ultrastable performance of this system. In the first we used a Mach-Zehnder interferometer with one mirror mounted on a loud speaker (Fig. 2) to measure the immunity to vibration of one of the internal components of the interferometer and in the second a Michelson interferometer was used to image an object(Fig. 5) while

#169402 - $15.00 USD Received 25 May 2012; revised 5 Jul 2012; accepted 9 Jul 2012; published 19 Jul 2012

the modulation frequency was swept to simulate much bigger amplitude vibrations than were possible in the first experiment. In both cases a 633 nm 6.5 mW He-Ne laser was used and a Bragg cell (optimum drive frequency of 40 MHz) was driven by a signal generator at 15 MHz unless otherwise stated.

In contrast to the previously presented heterodyne interferometer [2], the ultrastable configurations derive the LO signal not from the signal generator but from one of four pixels located near the centre of the MLC array. These four pixels have additional circuitry that allows the raw RF signal received by the photodiode to be routed off chip, where it is filtered using a 9 MHz to 15 MHz band pass filter before being fed to a 90° phase splitter and fed back to the MLC as the LO signals (seen in Fig. 2 and Fig. 5). This provides a LO signal that meets the conditions for Eq. (8). The external filtering does not contribute to the signal processing (because the on pixel filters provide much tighter 2 kHz filtering of the final signal) but are used to suppress out of band noise that might saturate the electronics.

The accuracy of this heterodyne interferometer using the MLC was explored in detail in previous work [2] for the conventional mode of operation. The ultrastable modification does not change this analysis and the interferometers presented here exhibit similar performance. Whilst in the previous implementation [2] the results were compared with homodyne interferograms, in this paper we can compared the ultrastable configuration with the same interferometer operating in the conventional heterodyne mode (using an LO signal derived from the signal generator driving the Bragg cell instead of RFout).

3.1. Mach-Zehnder interferometer with internal vibration

The Mach-Zehnder interferometer, seen in Fig. 2, is similar to the setup presented previously [2]. A spatial filter with a fixed pinhole and movable entry lens was included in the same arm as a Bragg cell. This permitted switching between heterodyne and homodyne modes of operation whilst retaining the same interferogram, and is used for easier visible alignment of the setup. The OPL difference between the two arms is constant (microphonics excepted) unless the loud speaker mounted mirror is driven. The motion of this mirror was monitored using a vibrometer (Polytec OFV-2570).

The position of the exit lenses was adjusted to produce a collimated reference beam and a weakly spherical object beam, generating circular fringe patterns at the MLC.

This arrangement allowed the ultrastable configuration to be tested with large internal OPL changes over a variety of frequencies simulating the effect of piston phase changes caused by vibrations, microphonics, temperature of other environmental factors.

3.1.1. The effect of the vibrating mirror

The RFout pixels have high frequency outputs, with DC being filtered out (I_{RF} from Eq. (2), seen in Fig. 1). With the optical arrangement shown in Fig. 2, the RFout signal is shown in Fig. 3(a) (bottom trace) with a 15 MHz reference signal (top trace). Even without driving the mirror, there is still some phase variance in the signal due to microphonics (Fig. 3(a), bottom left). Once the vibrating mirror mount is switched on, the RFout signal appears as noise, as the phase changes faster than can be captured (Fig. 3(b), bottom right).

3.1.2. Ultrastable operation

Using this system, as described above, circular fringe patterns were captured with a variety of vibrational amplitudes and frequencies produced by the loud speaker mounted mirror. Figure 4 shows the response to various vibration signals (top row) with the interferometer operating in conventional (middle row) and ultrastable modes (bottom row).

#169402 - $15.00 USD Received 25 May 2012; revised 5 Jul 2012; accepted 9 Jul 2012; published 19 Jul 2012

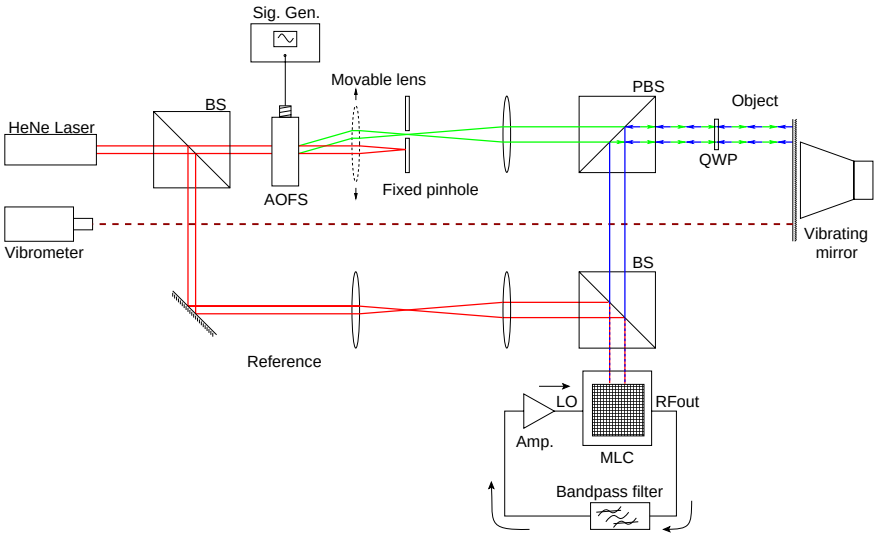

Fig. 2. Modified Mach-Zehnder interferometer. The interferometer uses a fixed pinhole and a movable lens in the same arm as a Bragg cell which permits the system to be change from heterodyne to homodyne operation whilst retaining the same interferogram. One mirror in this arm was mounted on a loud speaker, when this was driven it introduced large amplitude vibrations into the OPL. A Polytech vibrometer was used to measure the amplitude of vibration of this mirror.

The amount and frequency of the vibration induced on the subject mirror can be controlled. Three settings were chosen to show the ultrastable system working. The measurements captured, using the vibrometer, of the vibration velocity on the mirror are shown in Fig. 4(a) (no induced vibration), Fig. 4(b) (1 Hz square wave) and Fig. 4(c) (62 Hz sine wave). Even with the mirror mount turned off, there is still some vibration detected as seen in Fig. 4(a).

Figure 4(d) shows the fringe pattern captured using a signal from the signal generator as the local reference (Fig. 3 top trace) for the MLC, producing a standard heterodyne interferogram. Figure 4(e) and Fig. 4(f) are the captured image with the mirror mount vibrating at 1 Hz and 62 Hz respectively. A distorted fringe pattern is seen in Fig. 4(e) and no discernible fringe pattern can be seen in Fig. 4(f). It can be seen that the interferograms in the standard interferometer setup (stability mode off) are severely affected by the induced vibrations.

In the bottom row of Fig. 4, the interferometer is operating in the ultrastable mode and the interferograms can be seen to be unaffected by the induced vibrations. Images shown in Fig. 4(g), Fig. 4(h), Fig. 4(i) all use the RFout signal from a single centre pixel as the local reference for the MLC, with no vibration, 1 Hz vibration and 62 Hz vibration on the mirror mount respectively. All three ultrastable images show the fringe pattern clearly, but they do have a phase offset.

The immunity of the system to object beam vibration was demonstrated with the speaker driven from 18 Hz to 20 kHz over a wide range of amplitudes. The interferogram was found to be unchanged until the vibration velocity amplitude exceeding approximately 85 mm s^{-1} above which the fringes were progressively lost. At 62 Hz, this limit corresponds to sinusoidal motion with an amplitude of 0.22 mm. In terms of interferometer vibration sensitivity this is considered large, as discussed in the conclusion, but is considerably lower than the theoretical maximum amplitude of the system. It appears that at large amplitudes the motion of the mirror is not purely translational, therefore there are other modes of vibration produced (no longer pure

#169402 - $15.00 USD Received 25 May 2012; revised 5 Jul 2012; accepted 9 Jul 2012; published 19 Jul 2012

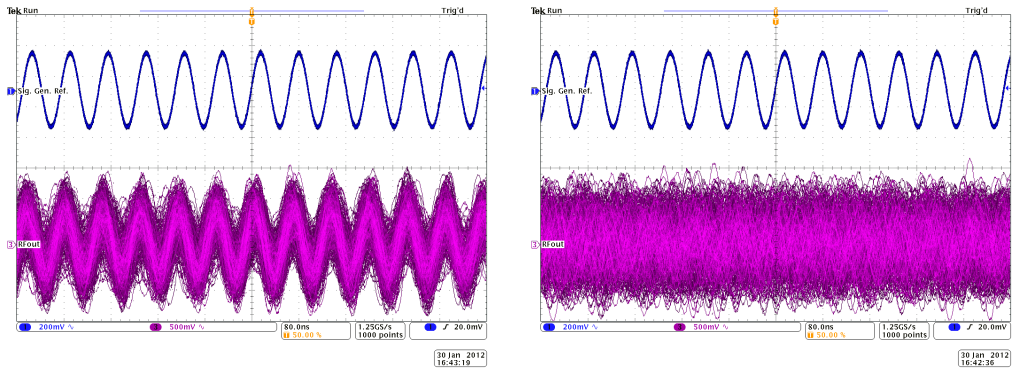

(a) (b)

Fig. 3. (top) The reference signal from a signal generator used to drive the Bragg cell in Fig. 2. (bottom) The signal captured from one of the RFout pixels (left) without driving the mirror and (right) with driving the mirror.

piston phase, i.e. vibration in the x-axis and y-axis as well as the z-axis), which effectively means that the wavefront of the object beam begins to have a spatially varying time dependence (i.e. $\phi_d(x,y) \rightarrow \phi_d(x,y,t)$ in Eq. (2)). A variety of different drivers were tried, all of which produced similar results at different frequency and amplitude limits.

3.2. Michelson interferometer

The Michelson interferometer is shown in Fig. 5. In this experiment the object was again mounted on a loud speaker which permitted the simulation of large vibrations or movement of the object with respect to the interferometer. Since it was found that the maximum amplitude of pure piston vibrations that the loud speaker could produce were significantly smaller than the theoretical maximum the system could compensate for (and smaller than in the Mach-Zehnder configuration due alignment issues stemming from the absence of the spatial filter), the ability of the system to handle larger vibration amplitudes is be demonstrated by introducing a variable offset frequency into the signal driving the Bragg cell.

The path lengths in this setup were carefully matched so that small variations in the fringes across the camera were detected. An initial image was then captured and subtracted from the subsequent object images to remove any residual phase distribution.

A test object consisting of a reflective amplitude grating (pitch 150 μm, height 140nm) was used as an object to facilitate testing (see inset Fig. 6).

This arrangement was intended to show the immunity to vibration of the object in the same manner as the previous experiment (§3.1) and the results were broadly similar with the limitation on the amplitude of vibration caused by the moving mirror mount failing to provide pure piston phase at high amplitudes.

Movement of the object produces changes in the piston phase that cause the modulation frequency to change. For example, a change of 1 Hz in the beat frequency is equivalent to a change in OPL of 1λ s^{-1}. As the local reference signal is derived from a pixel in the camera, it tracks this change and the MLC demodulates at the correct frequency regardless of the change.

The limitation of this arrangement occurs when the instantaneous modulation frequency (base frequency plus the changes produced by movement) exceeds the bandwidth of the MLC, the supporting electronics and devices. Thus it is possible to work out the maximum piston

#169402 - $15.00 USD Received 25 May 2012; revised 5 Jul 2012; accepted 9 Jul 2012; published 19 Jul 2012

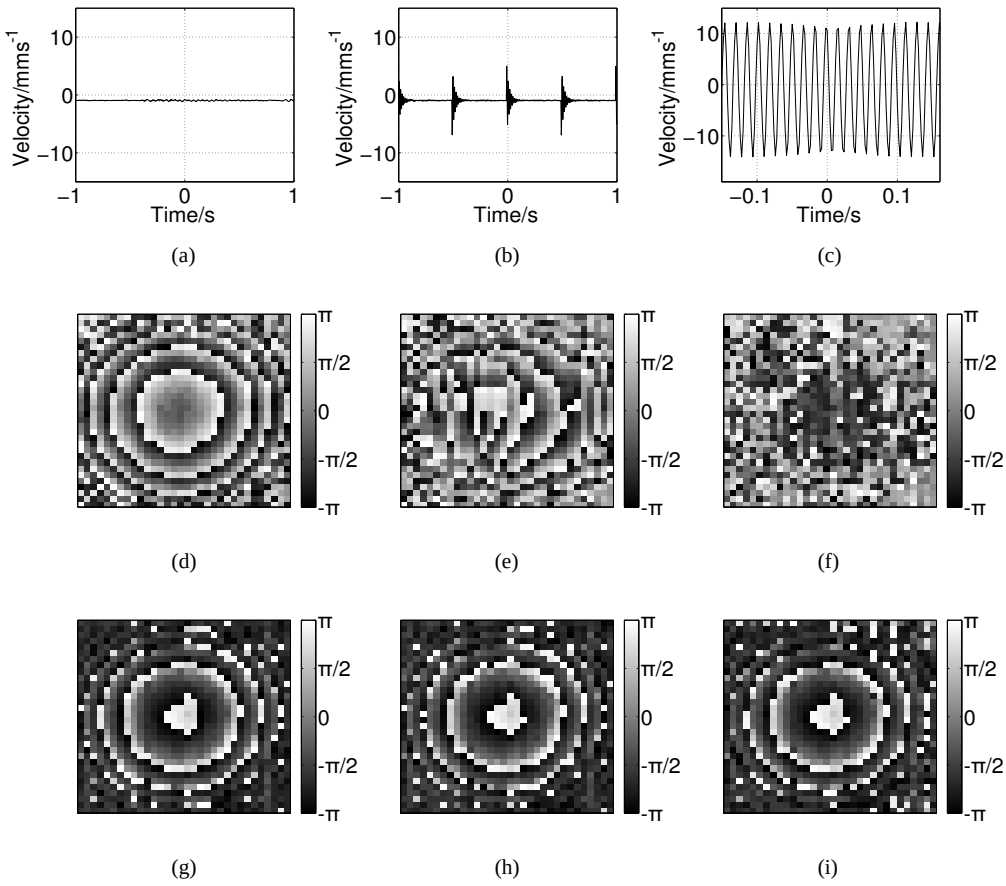

Fig. 4. (top) Traces of measured vibration velocity on the mirror mount using the vibrometer. (middle) Standard heterodyne interferogram images captured using an external signal as the LO, stability mode off. (bottom) Ultrastable heterodyne interferogram images captured using the RFout pixel feedback for the LO, stability mode on. Images taken with (a)(d)(g) no vibration induce, (b)(e)(h) 1 Hz square wave induced, (c)(f)(i) 62 Hz sine wave induce on the mirror mount. All fringe pattern images were taken with 20 averages.

phase shift that the system can tolerate by determining the bandwidth of the complete system. By introducing a change in the frequency driving the Bragg cell and sweeping it up and down until the image of the fringes deteriorates, the vibration tolerance can be determined.

The MLC presented in this paper has good frequency response from just above DC to above 15 MHz. Considering just the bandwidth limitation caused by the MLC and using a 633 nm light source, the system can tolerate a rate of change of OPL of $\sim$9.4 m s^{-1} (equivalent to an amplitude of sinusoidal vibration of 1.5 mm at 1 kHz).

In practice the limit is determined by the overall bandwidth of the system (see Fig. 1 and Fig.5) which includes the bandwidth limitations of the feedback electronics from the single pixel back to the array. For the purposes of practical measurement of the bandwidth, it also includes the limitations of the Bragg cell (Fig. 5).

Figure 6 shows interferograms taken with the complete system with the modulation fre-

#169402 - $15.00 USD Received 25 May 2012; revised 5 Jul 2012; accepted 9 Jul 2012; published 19 Jul 2012

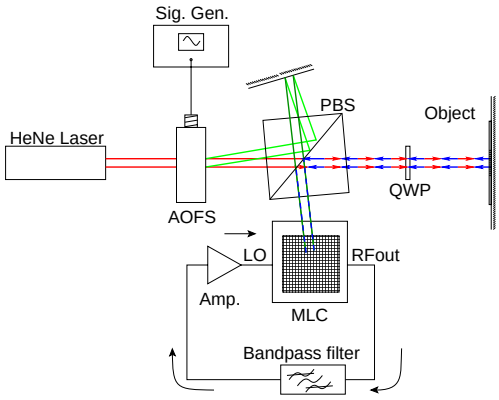

Fig. 5. Modified Michelson interferometer. The Bragg cell splits the beam into two orders with different frequencies that take different paths after going through a polarising beam-splitter. One beam is reflected off the object, and both beams are interfered when they pass through the beam splitter the second time.

quency varying from 11 MHz to 16 MHz. The object in this case is a metal surface relief grating. The clarity in the image depends on the strength of the RF signal (being fed-back as the local reference) as well the optical power incident on the detector (as both are mixed to output phase). The bandwidth limitation (and hence the vibration velocity) is dependant on the electronic filtering placed in the feedback loop, the low end the response for the Bragg cell and the upper end the response of the MLC.

The complete system shows good response over a bandwidth of 5 MHz corresponding to an object velocity tolerance of $\sim$3.1 m s^{-1}, equivalent to an amplitude of sinusoidal vibration of 0.5 mm at 1 kHz, or 8 mm at 62 Hz – significantly larger than the result measured in §3.1. Practically, the bandwidth could be increased by using a more sophisticated active filter or a lower frequency Bragg cell.

These images were taken at frame rates of up to 40 frames s^{-1}. The MLC is capable of frame rates of over 1 kHz, but the practical limitation in this case is determined by the capture rate of the data acquisition card used in this experiment.

4. Discussion and conclusion

Conventional homodyne and heterodyne interferometers detect OPL differences in the arms of the system, either by change in light intensity for homodyne systems or change in the relative phase of the modulated light for heterodyne systems. The prototype MLC outputs phase by mixing the detected light signal with a reference signal.

The ultrastable system described in this paper uses the raw signal captured by one pixel as a local reference, mixing it with the captured signal at each pixel in the camera. For a change of piston phase, the fringe pattern detected remains unchanged.

Unwanted vibrations can severely limit the performance of conventional interferometers, once the amplitude of the vibrations approaches an optical wavelength. By contrast, the ultrastable interferometer presented here is tolerant to vibrations of a much greater amplitude, experimentally demonstrated to be around $1.4\times10^5\,\lambda$ s^{-1} on a vibrating object and over $4.7\times10^6\,\lambda$ s^{-1} on a simulated moving object. Theoretically this prototype MLC could be used in a system tolerant to $15\times10^6\,\lambda$ s^{-1} of piston phase change.

Practical application experiments were carried out to characterise nanoscale gratings on a substrate. The profiles measured were comparable with images taken using an AFM and the

#169402 - $15.00 USD Received 25 May 2012; revised 5 Jul 2012; accepted 9 Jul 2012; published 19 Jul 2012

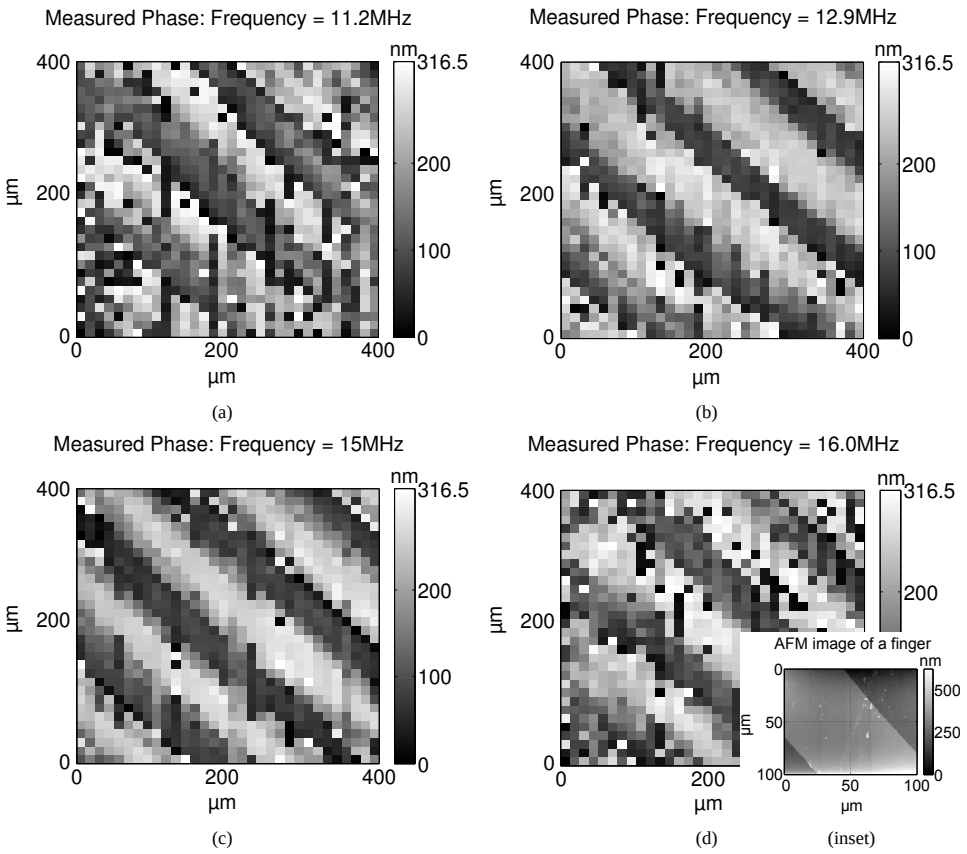

Fig. 6. Interferograms captured by the ultrastable Michelson interferometer as the modulation frequency was swept from 11MHz to 16MHz. The fringe pattern remains unchanged by the change in frequency because of the feedback from the RFout signal of one of the pixels to the LO input, meaning the MLC tracks the modulation frequency. At both ends of the frequency range, the noise is significantly increased because the signal is now at the edge of the system bandwidth. This is determined by the filters in the feedback path. The ability to handle this bandwidth is equivalent to immunity from piston phase change for an object moving at up to $3.1\,\mathrm{m\,s^{-1}}$. The inset shows an AFM image ($100\mu\mathrm{m}\times100\mu\mathrm{m}$) of the grating indicating the grating height (140 ± 20nm) which is in agreement with the measure phase in the interferograms.

experiment showed clear results with simulated constant vibration velocity of $3.0\,\mathrm{m\,s^{-1}}$. The measured practical boundary in this experiment is currently limited by both the Bragg cell operating range and the bandpass filters used for the RFout feedback. With optimisation, vibrational tolerance could be higher. The images of interferograms can be further improved with averaging to remove excess noise and systematic errors.

Considering this ultrastable system against a high speed acquisition where $3.0\,\mathrm{m\,s^{-1}}$ of OPL change is present. The phase image will be continuously changing but the image output from the MLC would remain relative to the RFout pixel, i.e. the same as long as the piston phase change remains uniform, all done without the need for averaging. For a high speed acquisition system with comparable immunity, for example 1 % accuracy, the entire frame would need to be captured before the OPL has changed by 1 % of the wavelength, 633 nm $\rightarrow\sim$6 nm. With

#169402 - $15.00 USD Received 25 May 2012; revised 5 Jul 2012; accepted 9 Jul 2012; published 19 Jul 2012

$3.0\,\mathrm{m\,s^{-1}}$ of constant OPL change, the acquisition time for the entire frame would need to be less than $\sim$2 ns which would require an extremely complex system and still require averaging. Of course, this becomes more of a challenge if a higher accuracy is required and for high resolution systems, but is offset by higher averaging (which can bring in its own problems). The MLC can be scaled up to for higher resolutions without any problems as the vibration immunity of the system does not depend on the acquisition speed, and still retains the ability for averaging (for removal of tilt or noise).

The ultrastable system presented can be useful for many different applications where accuracy over time is important. As seen in Fig. 3(a) and Fig. 4(a), even in steady conditions, environmental factors can affect unstabilised interferometers. The combination of the integrated camera with the ultrastable setup is ideal for medical, industrial and academic applications where subject characterisation is the emphasis.

Table 1. Table summarising the immunity to vibration for the ultrastable interferometer. The right hand columns indicate the amplitude of sinusoidal vibration at various frequencies.

	V_{vib}	$A_{0.5\mathrm{Hz}}$	$A_{10\mathrm{Hz}}$	$A_{62\mathrm{Hz}}$	$A_{1\mathrm{kHz}}$
Measured	$85.0\,\mathrm{mm\,s^{-1}}$	27 mm	1.3 mm	220 μm	14 μm
Simulated	$3.1\,\mathrm{m\,s^{-1}}$	1 m	50 mm	8 mm	0.5 mm
Theoretical	$9.4\,\mathrm{m\,s^{-1}}$	3 m	150 mm	24 mm	1.5 mm

ISO2631 guidelines state that the maximum vibration ampltidue should be 6.4um and 12.7um for of?cse and a workshos respectively. Large seismic shocks from earthquakes have peak amplitudes at 0.5 Hz [19, 20] and can reach amplitudes of 1 m, which is still within the simulated stability limit of this interferometer.

Table 1 summarises the limits of immunity to piston phase change for the current system. For comparison, typical vibration for ambient and shock vibrations in buildings displacements at 10 Hz are around 25 μm and 253 μm respectively [16], and for a moving car (30 kph) is around 220 μm [17]. ISO2631 guidelines state that the maximum vibration ampltidue should be 6.4 μm and 12.7 μm (at 10 Hz) for an office and a workshop respectively [18]. Large seismic shocks from earthquakes have peak amplitudes at 0.5 Hz [19, 20] and can reach amplitudes of $\sim$1 m, which is still within the simulated stability limit of the interferometer.

It might be assumed that at low frequencies (lower than the frame rate of the camera used to capture the interferogram) that conventional interferometers might be operated by just taking quick snapshots faster than the period of vibration. However at high amplitudes of vibration, the relevant time-scale is λ/V_{vib} (or the time taken for the path length change by approximately one wavelength). For the examples above correspond to microseconds or less, requiring extremely high frame rates. The ultrastable interferometer presented here has no such requirement on the frame rate for piston phase changes.

This shows that the system is practically immune to most levels of vibration normally encountered and makes this system suitable for operation in applications or environments not normally consider ideal for interferometers such as workshops, offices, factories or operating theatres.

#169402 - $15.00 USD Received 25 May 2012; revised 5 Jul 2012; accepted 9 Jul 2012; published 19 Jul 2012